Supporting Information

Investigating the Backbone Conformation and Configuration Effects for Donor−Acceptor Conjugated Polymers with Ladder−Type Structures Synthesized Through Aldol Polycondensation

Yen-Wen Huang,[a] *Yan-Cheng Lin,*[a,b], *Jian-Sian Li,*[a,b] *Wen-Chang Chen,*[a,b]* *and Chu-Chen Chueh,*[a,b,]*

[a] Department of Chemical Engineering, National Taiwan University, Taipei 10617, Taiwan

[b] Advanced Research Center for Green Materials Science and Technology, National Taiwan University, Taipei 10617, Taiwan

*Corresponding authors: cchueh@ntu.edu.tw; chenwc@ntu.edu.tw

KEYWORDS. Donor-accepter conjugated polymers; ladder-type structures; backbone conformation and configuration; field-effect transistors

Characterizations

SEC from Enshine SUPER CO-150 with PS gel columns (Stryagel HR 2 and stryragel 4) and THF as eluent at 40 °C, 1.0 mL min^{-1} was used to evaluate the molecular weight of the polymers. The calibration was made by standard PS to acquire M_n, M_w, and $Đ$ values of the polymers. Hitachi U-4100 spectrophotometer was adopted to obtain solution and thin-film UV−vis absorption spectra. Solution with a concentration of 0.03 mg/mL and spin-coated films on quartz substrate were used for measurement of UV−vis absorption. To measure solubility of the polymers in chlorobenzene, 5 mg of polymers were blended with 0.1 mL of chlorobenzene and filtered. The insoluble fraction was removed by syringe filter and the solution was diluted (400 times in volume) and its UV−vis absorption intensity was compared with a solution made of the same polymer with a concentration of 0.03 mg/mL. Finally, the solubility was calculated according to the Lambert-Beer law at 25 °C. Nanoscope 3D Controller atomic force microscopy (AFM, Digital Instruments) under

tapping mode was applied to characterize the surface morphology at room temperature for the spin-coated polymer films. Elastic moduli representing the surface mechanical properties of the polymers were characterized and estimated by Dimension Icon, Bruker conducted in the PeakForceTM tapping mode. The spring constant of the cantilevers ranges from 5−42 N m^{-1} with standard silicon tips (OTESPA) and the applied force was in a range between 5−300 nN. The tip oscillated at a frequency of 2 kHz below the cantilever resonant frequency (300 kHz). The thin-film samples are prepared on a ODTS-modified silicon wafer, and the elastic moduli of the polymer films were fitted by the DMT model that is suitable to low adhesion and small tip radii. GIXD measurements were conducted on beamline 17A1 in National Synchrotron Radiation Research Center, Taiwan. An X-ray wavelength of 1.322 Å and an incident angle at 0.12° were used. The FET characteristics of the polymer films were characterized using a Keithley 4200-SCS semiconductor parameter analyzer (Keithley Instruments Inc.) in an N_2-filled glovebox. For a transferred film supported on a PDMS substrate, the crack-onset strain was measured under a Microtech optical microscope.

Material Synthesis and Characterization

9-(iodomethyl)nonadecane was synthesized according to the methods reported in the literature. The synthetic procedures for monomers (**M1** and **M2**) were adopted from the previous literature with sligh modifications, as displayed in **Scheme S1**.[1-4]

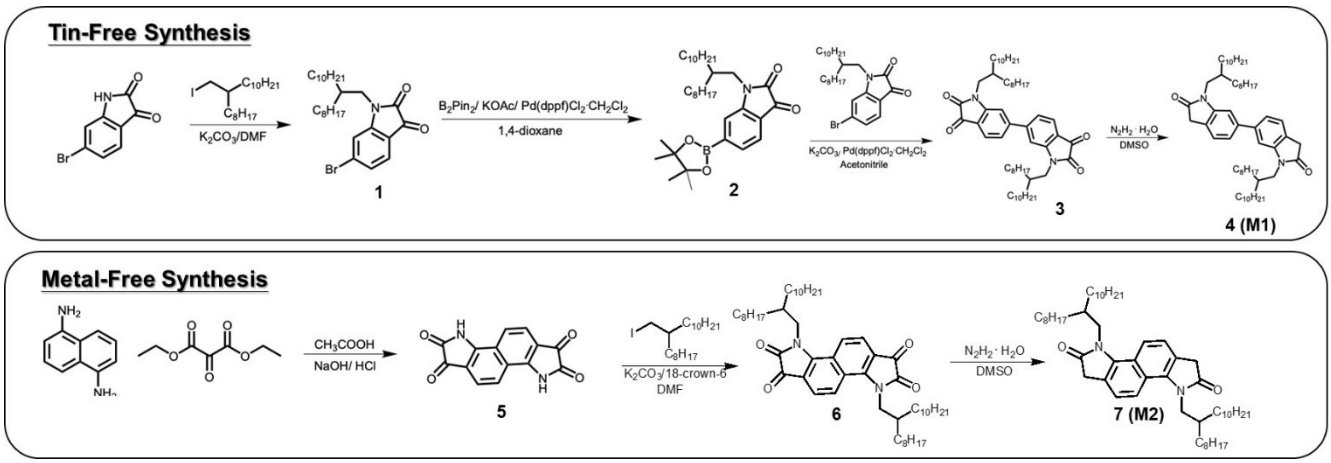

Scheme S1. Synthetic routes for the monomers with bis-isatin core (**M1**) and fused bis-isatin core (**M2**).

***Synthesis of 6-bromo-1-(2-octyldodecyl)indoline-2,3-dione* (1)**

6-bromoindoline-2,3-dione (3 g, 1.0 eq.) and potassium carbonate (2.55 g, 1.4 eq.) were dissolved in dry *N,N*-dimethylformamide (DMF) (80 mL) added through syringe in a dry flask under nitrogen atmosphere. 9-(iodomethyl)nonadecane(2.75 g, 1.2 eq.) was injected and the mixture was stirred overnight after the temperature was raised to 100 ^{o}C for 18 hrs. The mixture was extracted by brine and ethyl acetate, and the organic phase was collected and dried over magnesium sulfate to acquire dark brown oil. Finally, the mixture was purified by column chromatography using ethyl acetate: hexane (1:10) as the eluent to obtain the target compounds as brown oil (5.20 g, 90 %). ^{1}H NMR (400 MHz, $CDCl_3$), δ (ppm): 7.44 (d, 1H), 7.26 (s, 1H), 7.03 (s, 1H), 3.55 (d, 2H), 2.02 (s, 1H), 1.23 (br, 28H), 0.85 (tr, 9H).

***Synthesis of 1-(2-octyldodecyl)-6-(4,4,5,5-tetramethyl-1,3,2-dioxaborolan-2-yl)indoline-2,3-dione* (2)**

6-bromo-1-(2-octyldodecyl)indoline-2,3-dione (3.0g, 1.0 eq.), bis(pinacolato)diboron (1.80g, 1.2 eq.), potassium acetate (1.70g, 3.0 eq.), [1,1′-bis(diphenylphosphino)ferrocene]dichloropalladium (II) (110.6 mg, 0.67 mM) were sealed in a microwave vial under nitrogen atmosphere. 1,4-Dioxane (2 mL) was injected through syringe and the reactant was heated to 120 °C for 50 mins in a microwave reactor. The mixture was extracted by brine and ethyl acetate for three time, and the organic phase was collected and dried over magnesium sulfate. The mixture was finally purified by column chromatography using DCM as the eluent to obtain the target compound as orange solid powers (1.64 g, 50 %). ^{1}H NMR (400 MHz, $CDCl_3$), δ (ppm): 7.53 (s, 2H), 7.22 (s, 1H), 3.58 (d, 2H), 2.02 (s, 1H),1.34 (s, 12H), 1.22 (br, 28H), 0.85 (tr, 9H).

***Synthesis of 1,1'-bis(2-octyldodecyl)-[6,6'-biindoline]-2,2',3,3'-tetraone* (3)**

1-(2-Octyldodecyl)-6-(4,4,5,5-tetramethyl-1,3,2-dioxaborolan-2-yl)indoline-2,3-dione (3.50 g, 1.1 eq.), [1,1′-bis(diphenylphosphino)ferrocene]dichloropalladium (II) (60 mg), and 6-bromo-1-(2-octyldodecyl)indoline-2,3-dione (2.14g, 1.0 eq.) were sealed in a microwave vial under nitrogen atmosphere. Potassium carbonate (800g, 0.4 eq.) was dissolved in a minimum amount of water and injected into the vial through syringe. Acetonitrile (4 mL) was injected through syringe and was heated to 80 °C for 60 mins in a microwave reactor. The mixture was extracted by brine and ethyl acetate for three time, and the organic phase was collected and dried over magnesium sulfate. The mixture was finally purified by column chromatography using ethyl acetate: hexane (1:10) as the eluent to obtain the target compound as red solid powders (1.90 g, 35 %). ^{1}H NMR (400 MHz, $CDCl_3$), δ (ppm): 7.70 (d, 2H), 7.28 (d, 2H), 6.99 (s, 2H) 3.65 (d, 4H), 1.86 (s, 2H), 1.40-1.05 (br, 56H), 0.85 (s, 18H).

***Synthesis of 1,1'-bis(2-octyldodecyl)-[6,6'-biindoline]-2,2'-dione* (4 or M1)**

1,1'-Bis(2-octyldodecyl)-[6,6'-biindoline]-2,2',3,3'-tetraone (1.90g) was dissolved in hydrazine monohydrate (25 mL) and DMSO (25 mL) under nitrogen protection. The mixture was refluxed at 140 °C for 30 hrs and cooled to room temperature. The mixture was then poured into brine and extracted with ethyl acetate for three time. The organic phase was collected, dried by magnesium sulfate, and purified by column chromatography using ethyl acetate: hexane (1:5) as the eluent to obtain the target compounds as light brown oil (1.70g, 92 %).^{1}H NMR (400 MHz, $CDCl_3$), δ (ppm): 7.29 (d, 2H), 7.19 (d, 2H), 6.95 (s, 2H) 3.62 (d, 4H), 3.55 (d, 4H),1.86 (s, 2H), 1.40-1.05 (br, 56H), 0.85 (s, 18H). ^{13}C NMR (400 MHz, $CDCl_3$) δ (ppm): 175.31,

145.69, 141.28, 124.52, 123.85, 120.86, 107.37, 60.30, 44.47, 36.32, 35.45, 31.78, 31.57, 29.97, 29.54, 29.25, 26.46, 22.58, 14.01. Anal. calc'd. for [$C_{56}H_{92}N_2O_2$] C, 81.49; H, 11.24 N, 3.29. Found: C, 79.35; H, 11.45; N, 4.03.

Synthesis of 3,8-dihydroindolo[7,6-g]indole-1,2,6,7-tetraone **(5)**

Naphthalene-1,5-diamine (3.0 g, 1.0 eq.) was dissolved and refluxed in glacial acetic acid (40 mL) under nitrogen atmosphere, and 12 mL of diethyl 2-oxomalonate in 36 mL of acetic acid was dropwise added into the mixture over 30 mins. The resulting mixture was further refluxed for 20 hrs. After removing the acetic acid under vacuum, the brown solid was dissolved in 1 M NaOH and refluxed for 8 hrs with air sparging. The mixture was cooled to 0 °C before adding 6 M HCl and stirred for another 20 mins. The precipitate was collected by filtration and washed with cold water to acquire dark purple solid powders (5.26 g). The dark purple solid powders were used subsequently without further purification. ^{1}H NMR (400 MHz, d_6-DMSO), δ (ppm): 11.79 (s, 2H), 7.81(d, 2H), 7.62 (d, 2H).

Synthesis of 3,8-bis(2-octyldodecyl)-3,8-dihydroindolo[7,6-g]indole-1,2,6,7-tetraone **(6)**

3,8-Dihydroindolo[7,6-g]indole-1,2,6,7-tetraone (300 mg g, 1.0 eq.) and potassium carbonate (400 mg, 3.0 eq.) were dissolved in dry *N,N*-dimethylformamide (DMF) (10 mL) added through syringe in a dry flask under nitrogen protection. 9-(Iodomethyl)nonadecane(1.01 g, 2.2 eq.) was injected and the mixture was stirred overnight after the temperature was raised to 70 ^{o}C for 30 mins. The reaction temperature was further raised to 100 ^{o}C for another 5 hrs, and allowed to be cooled to room temperature. The solvent was subsequently

removed with a rotary evaporator. The mixture was first passed through a silica gel column with DCM as eluent to acquire the crude products. Then, the mixture was purified through column chromatography using a gradient eluent of ethyl acetate: hexane 1:20 to 1:5 to obtain the target compounds as a blue solid powders (70 mg, 10 %). ^{1}H NMR (400 MHz, $CDCl_3$), δ (ppm): 7.97 (d, 2H), 7.63 (d, 2H), 4.14 (d, 2H), 1.88 (s, 2H), 1.20 (br, 56H), 0.85 (tr, 18H). ^{13}C NMR (400 MHz, $CDCl_3$) δ (ppm): 182.62, 159.20, 152.28, 127.32, 119.97, 119.85, 116.24, 47.51, 37.49, 31.80, 31.74, 30.98, 29.85, 29.49, 26.09, 22.55,14.00.

Synthesis of 3,8-bis(2-octyldodecyl)-1,3,6,8-tetrahydroindolo[7,6-g]indole-2,7-dione **(7 or M2)**

3,8-Bis(2-octyldodecyl)-3,8-dihydroindolo[7,6-g]indole-1,2,6,7-tetraone (240 mg) was dissolved in hydrazine monohydrate (25 mL) and DMSO (25 mL) under nitrogen atmosphere. The mixture was refluxed at 140 °C for 18 hrs and cooled to room temperature. The mixture was then poured into brine and extracted with ethyl acetate for three time. The organic phase was collected, dried by magnesium sulfate, and purified by column chromatography using ethyl acetate:hexane (1:15) as the eluent to obtain the target compounds as light yellow solid powders (175 mg, 75 %).^{1}H NMR (400 MHz, $CDCl_3$), δ (ppm): 7.94 (d, 2H), 7.36 (d, 2H), 4.16 (d, 4H), 3.66(s, 4H),1.97 (s, 2H), 1.40-1.05 (br, 56H), 0.85 (s, 18H). ^{13}C NMR (400 MHz, $CDCl_3$) δ (ppm): 176.77, 140.61, 121.82, 121.47, 120.18, 116.16, 46.89, 36.13, 35.41, 31.79, 31.16, 29.92, 29.50, 29.43, 26.22, 22.55, 13.96. Anal. calc'd. for [$C_{54}H_{90}N_2O_2$] C, 81.14; H, 11.35; N, 3.50. Found: C, 80.01; H, 11.79; N,3.46.

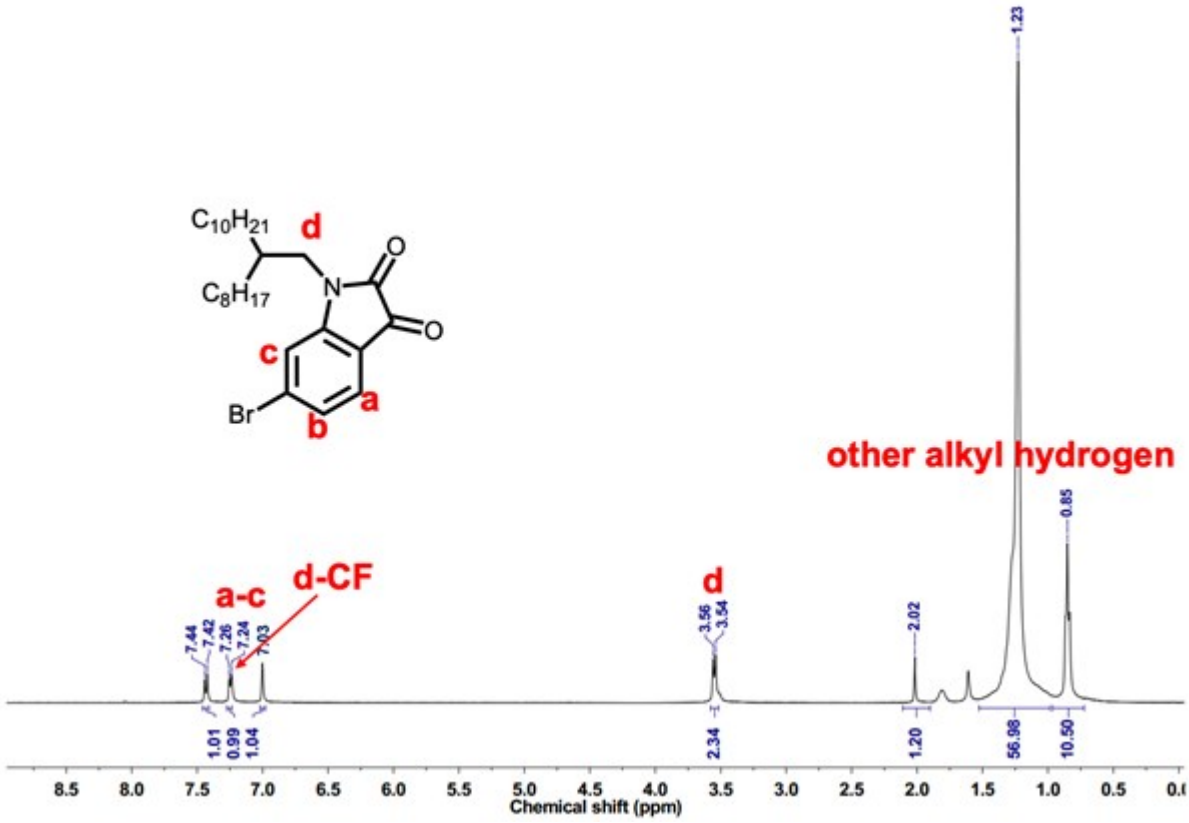

Figure S1. ^{1}H NMR of compound **1** in $CDCl_3$.

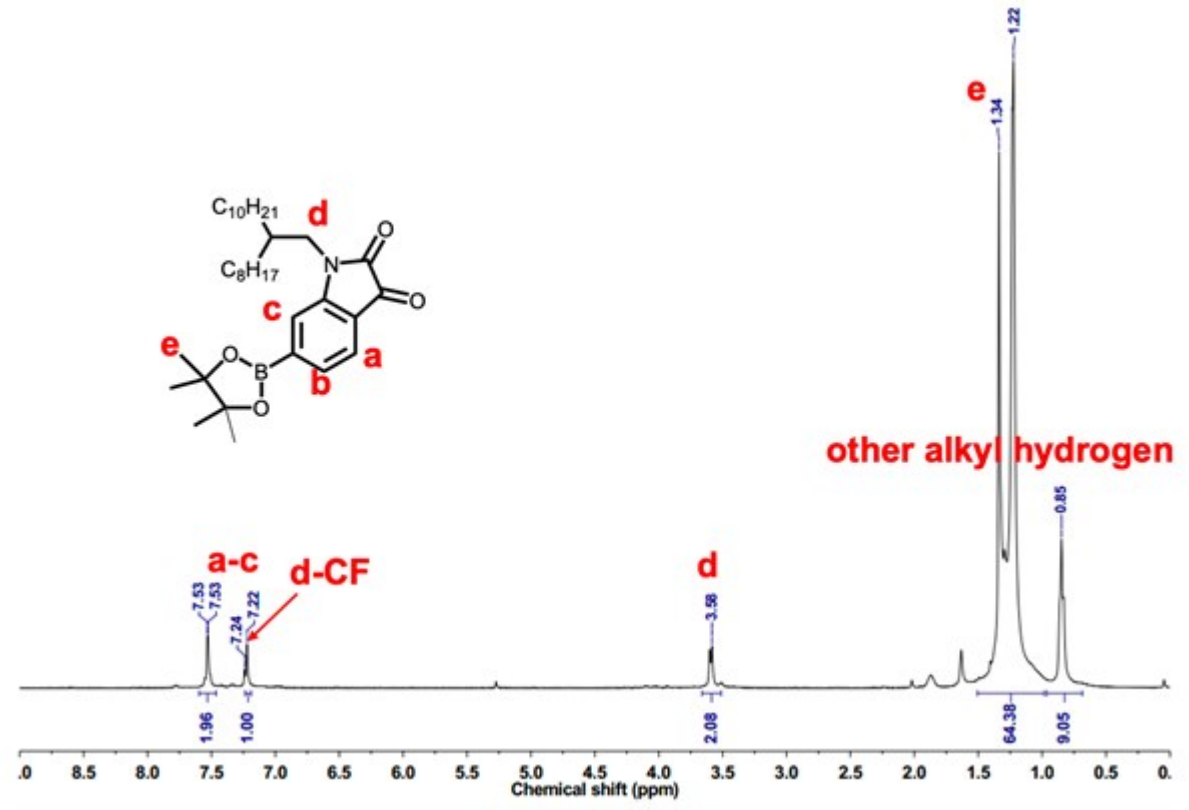

Figure S2. ^{1}H NMR of compound **2** in $CDCl_3$.

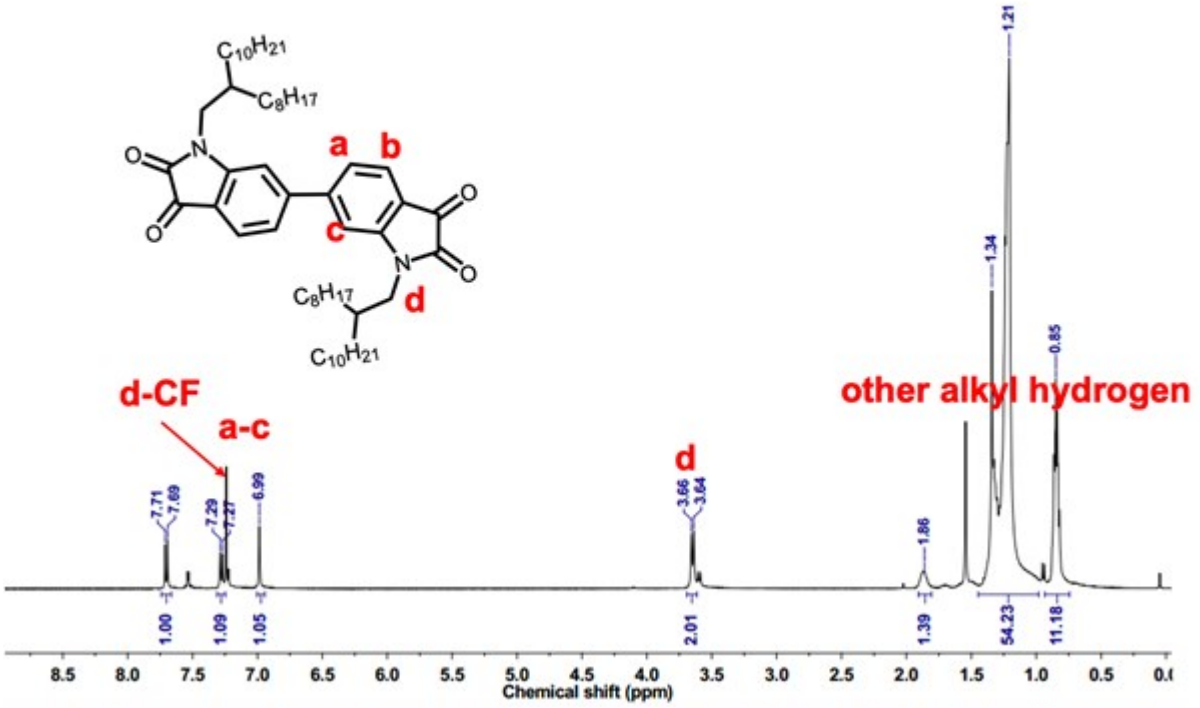

Figure S3. ^{1}H NMR of compound **3** in $CDCl_3$.

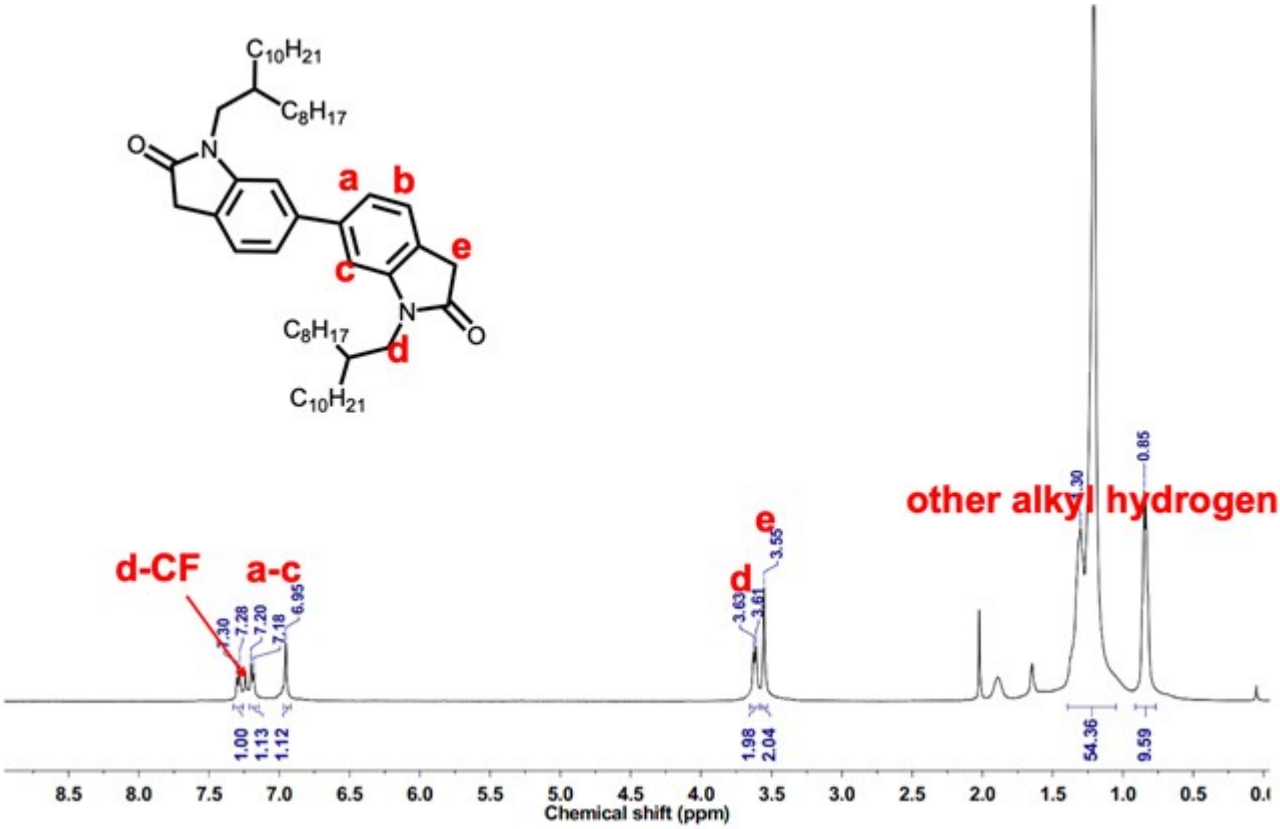

Figure S4. ^{1}H NMR of compound **4** in $CDCl_3$.

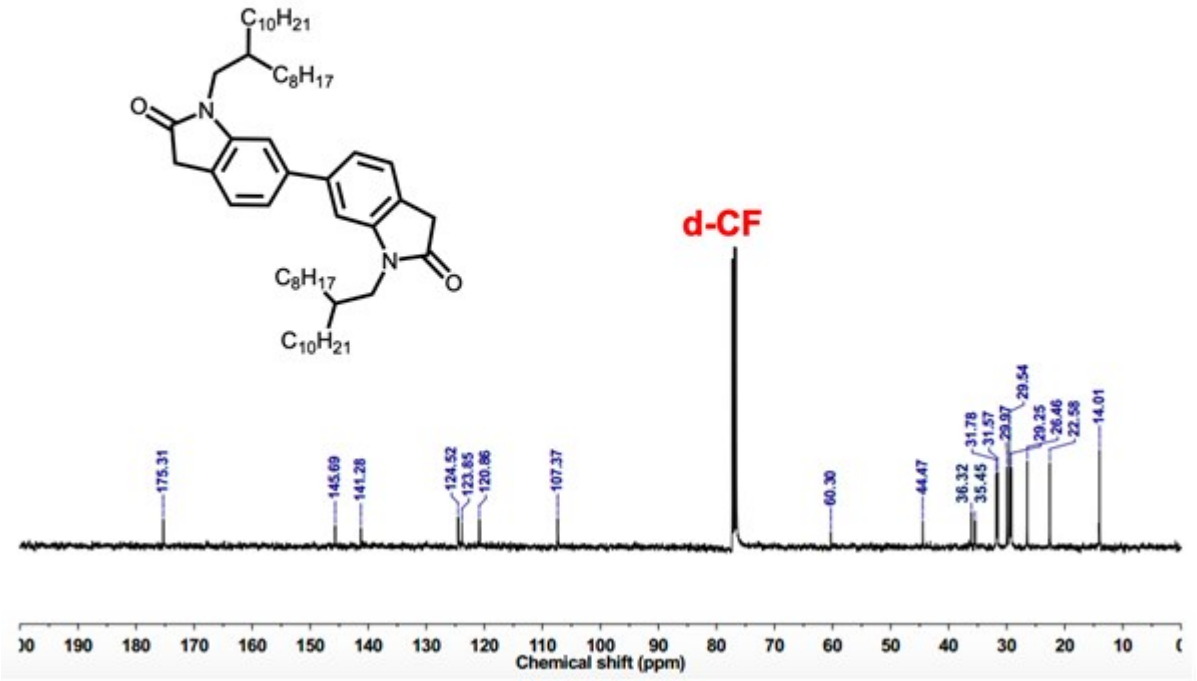

Figure S5. ^{13}C NMR of compound **4** in $CDCl_3$.

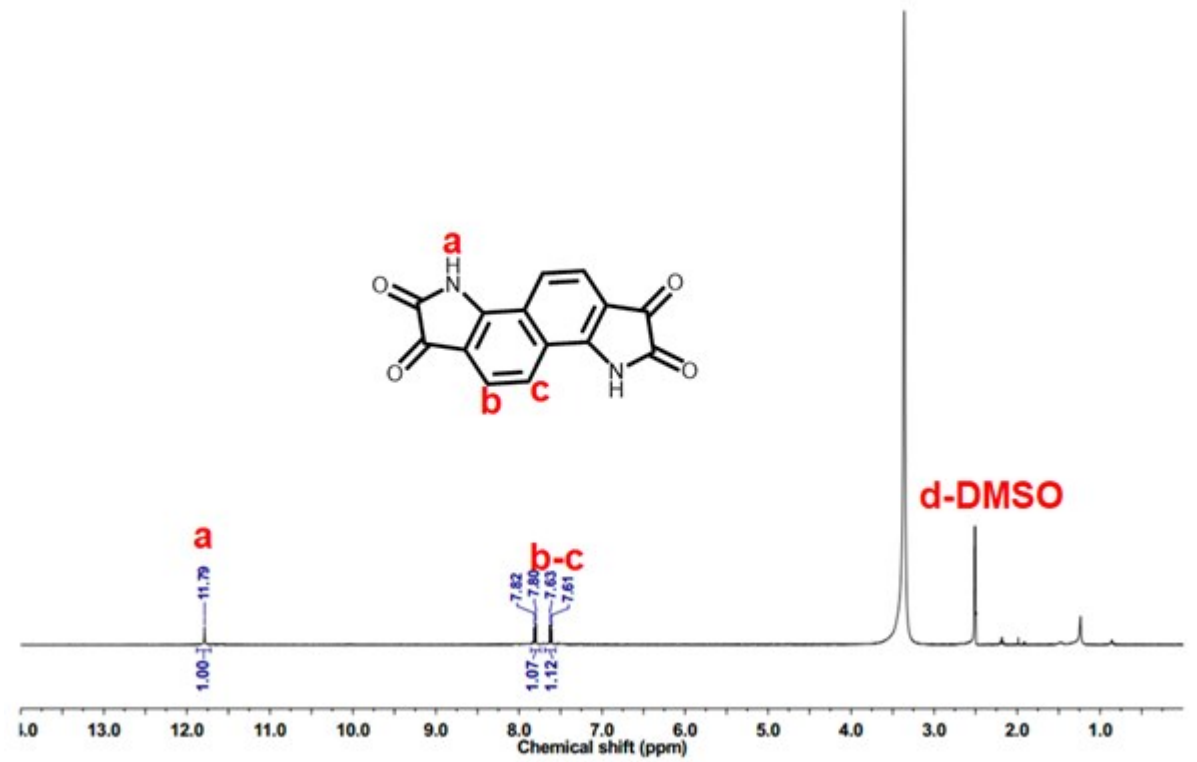

Figure S6. ^{1}H NMR of compound **5** in d-DMSO.

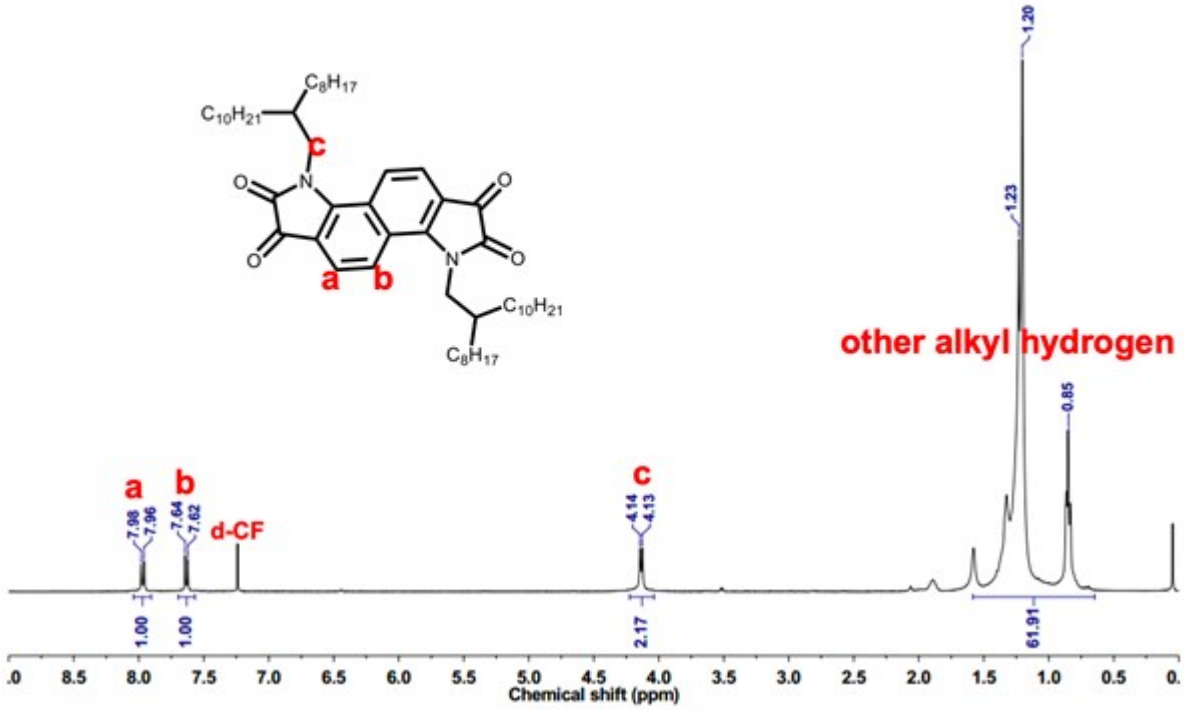

Figure S7. ^{1}H NMR of compound **6** in $CDCl_3$.

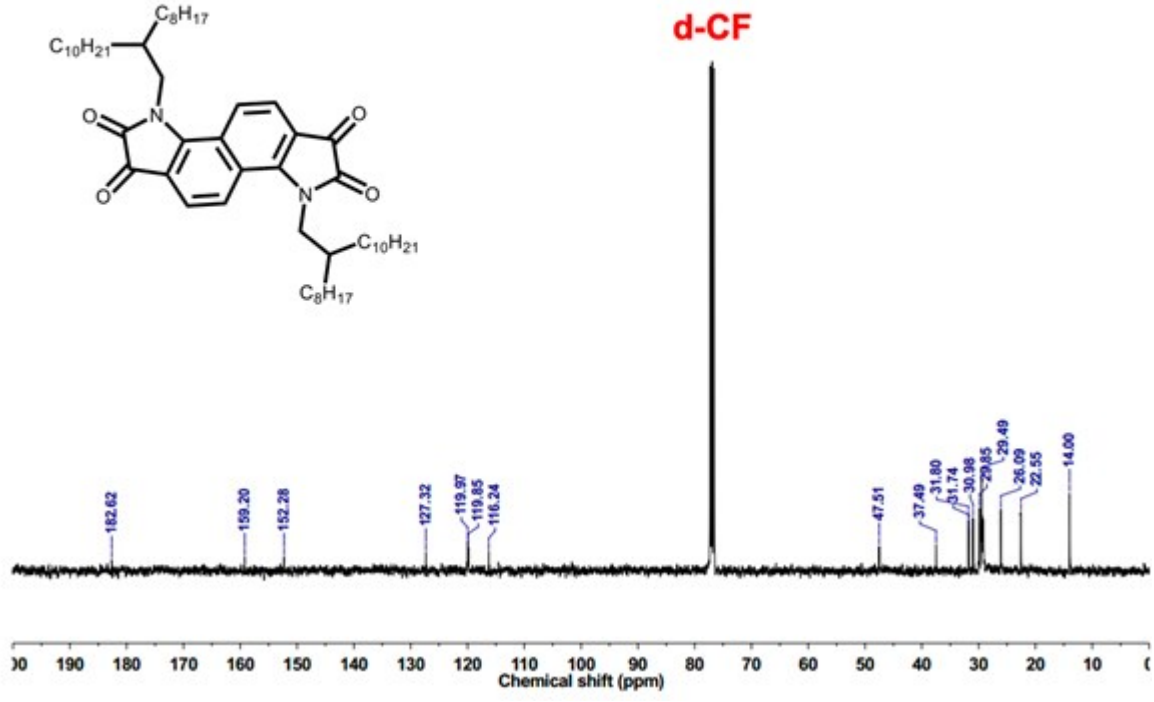

Figure S8. ^{13}C NMR of compound **6** in $CDCl_3$.

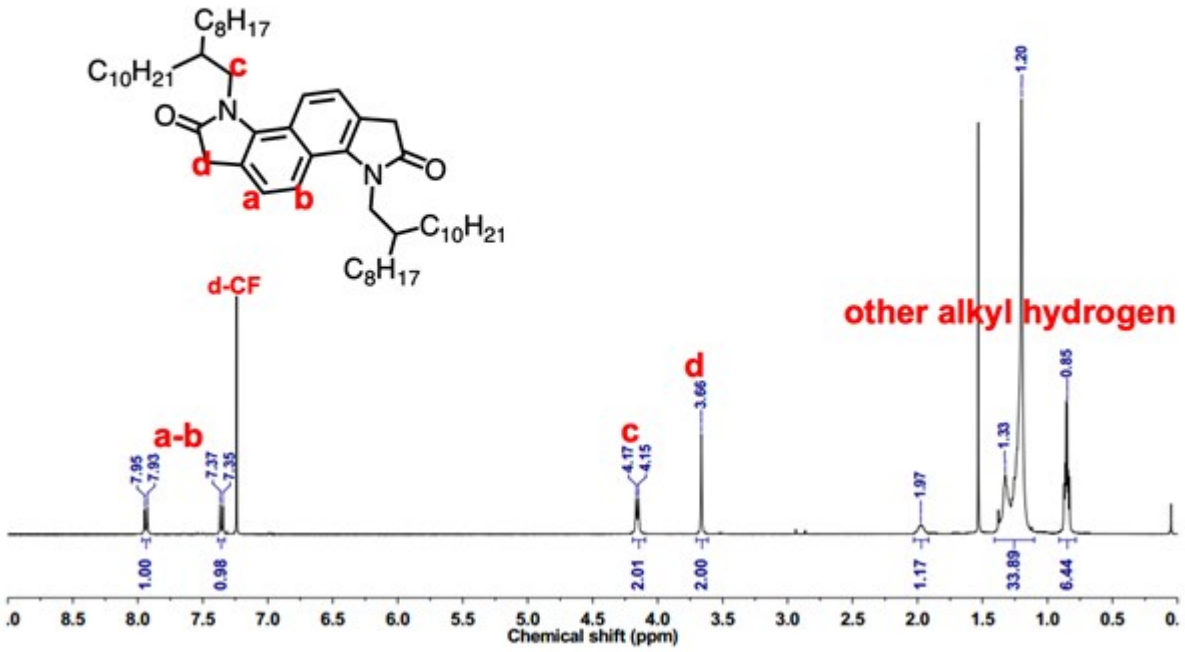

Figure S9. ^{1}H NMR of compound **7** in $CDCl_3$.

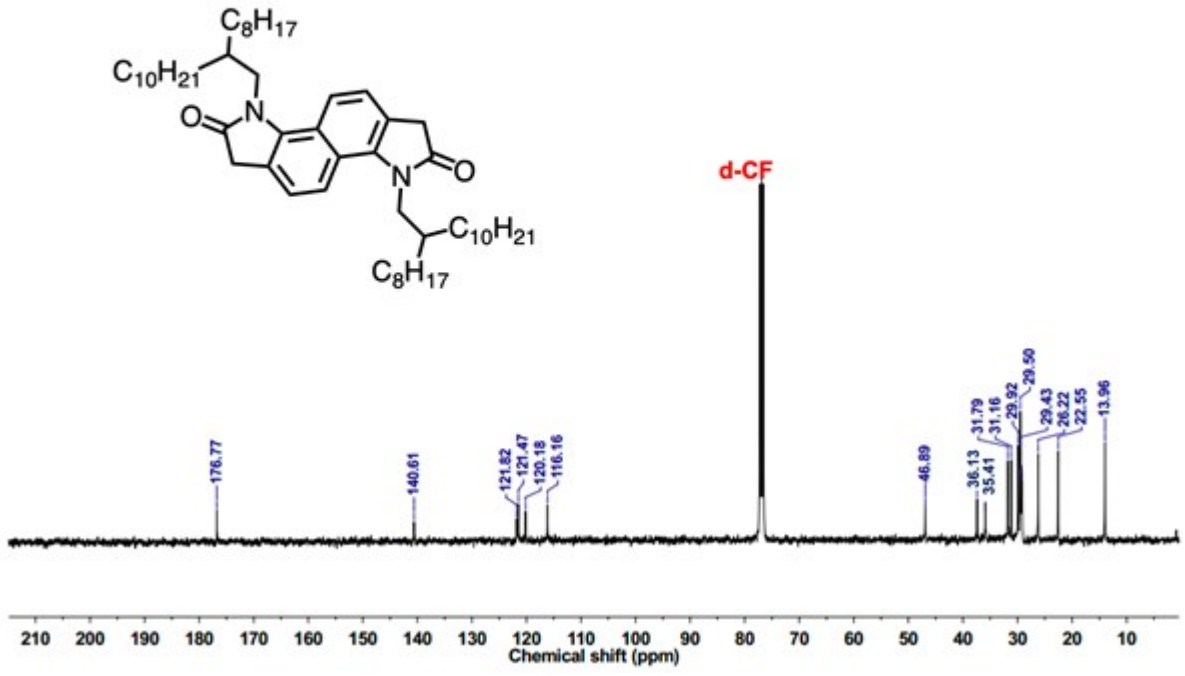

Figure S10. ^{13}C NMR of compound **7** in $CDCl_3$.

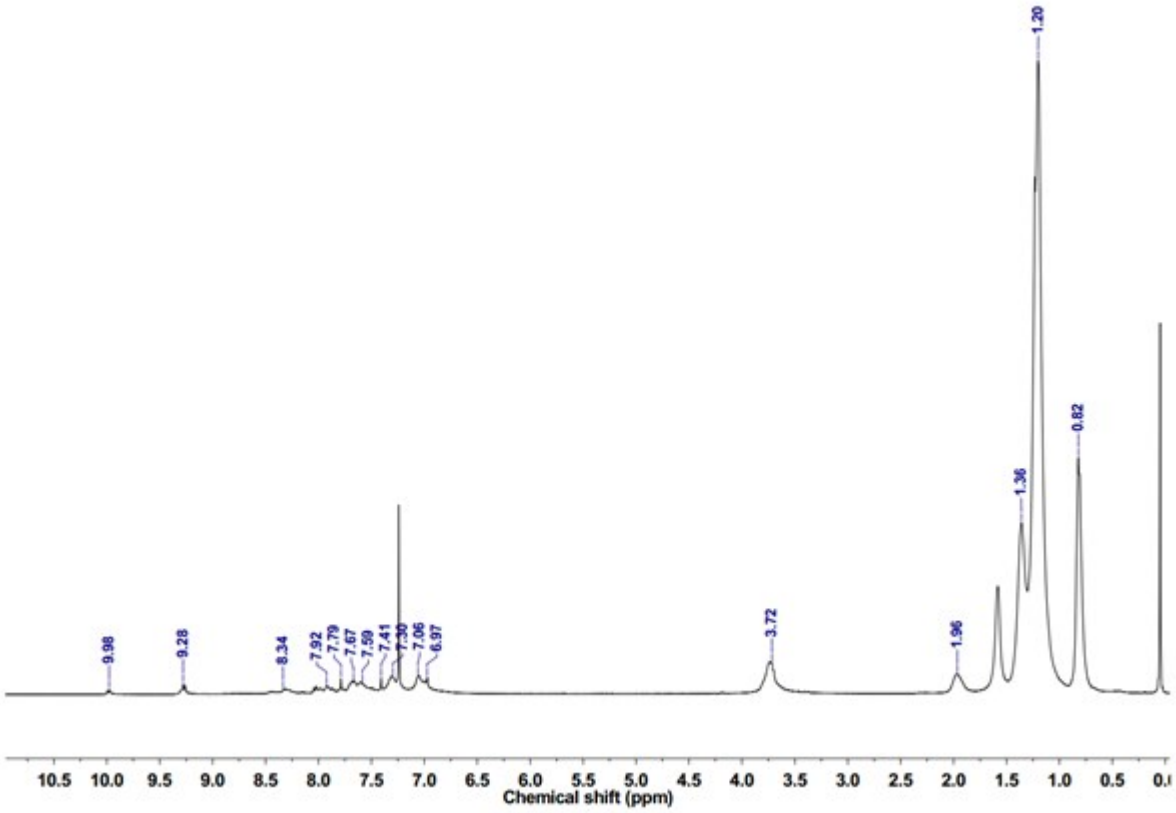

Figure S11. ^{1}H NMR of **P1** in $CDCl_3$.

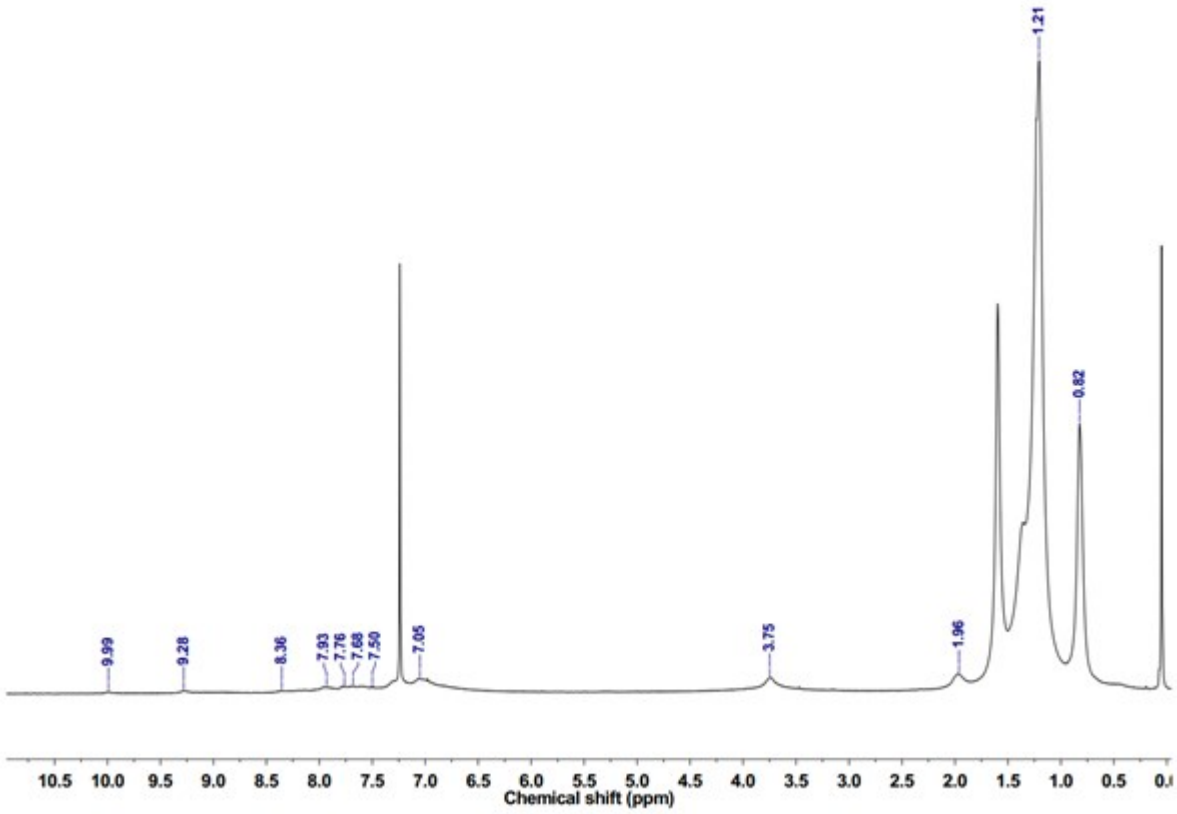

Figure S12. ^{1}H NMR of **P2** in $CDCl_3$.

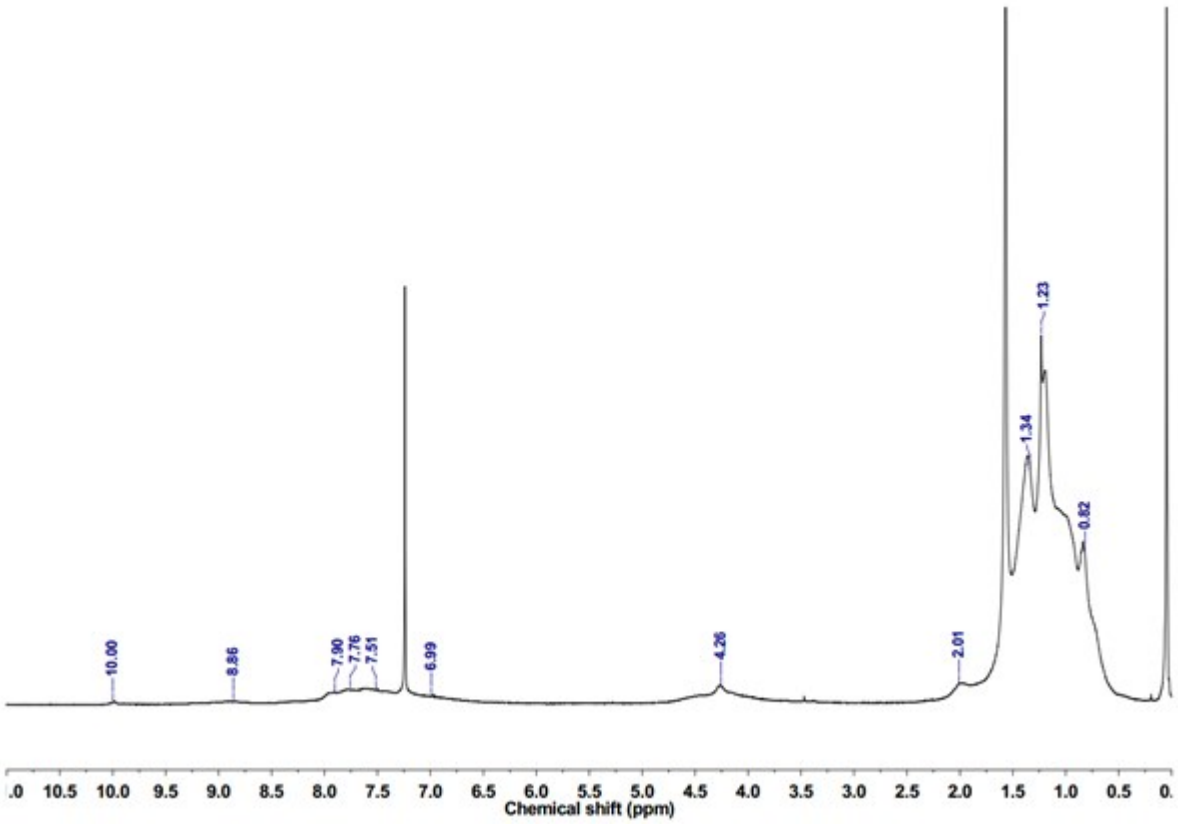

Figure S13. ^{1}H NMR of **P3** in $CDCl_3$.

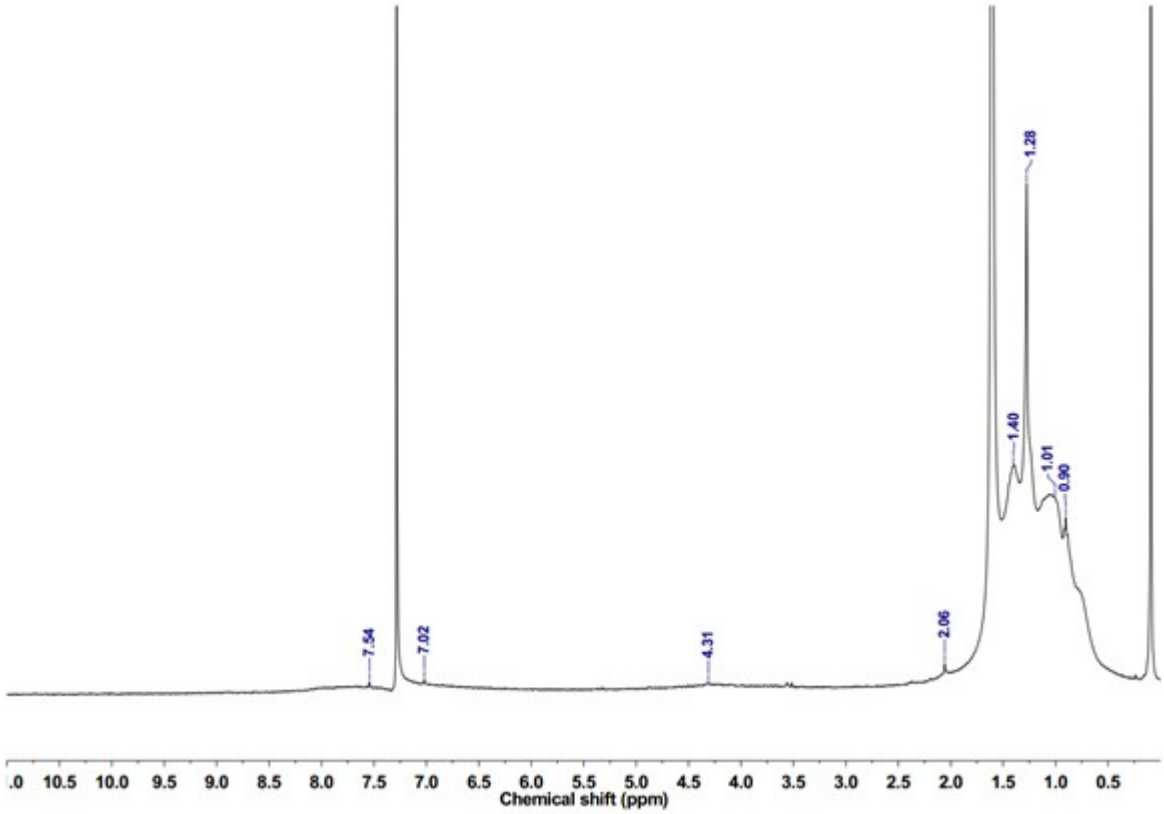

Figure S14. ^{1}H NMR of **P4** in $CDCl_3$.

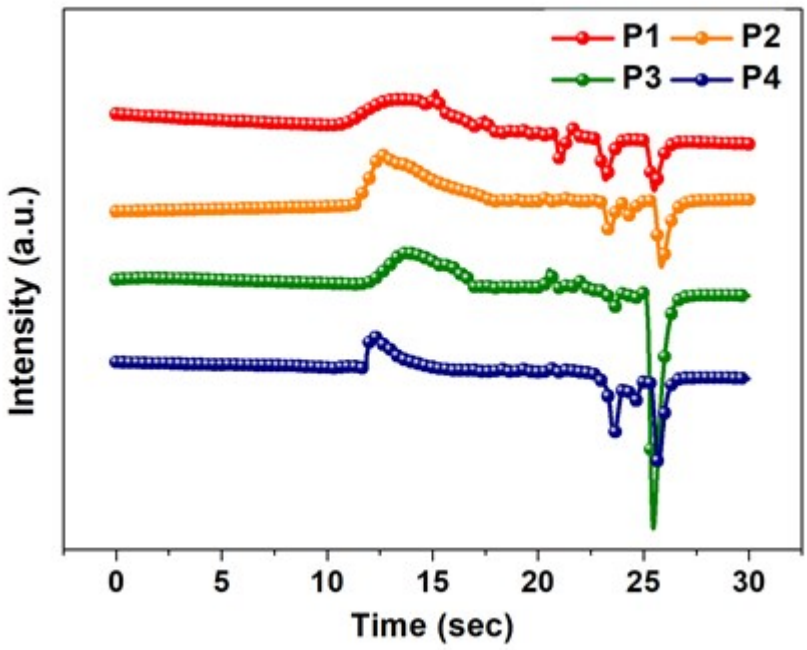

Figure S15. SEC profiles of **P1-P4** using THF used as the eluent.

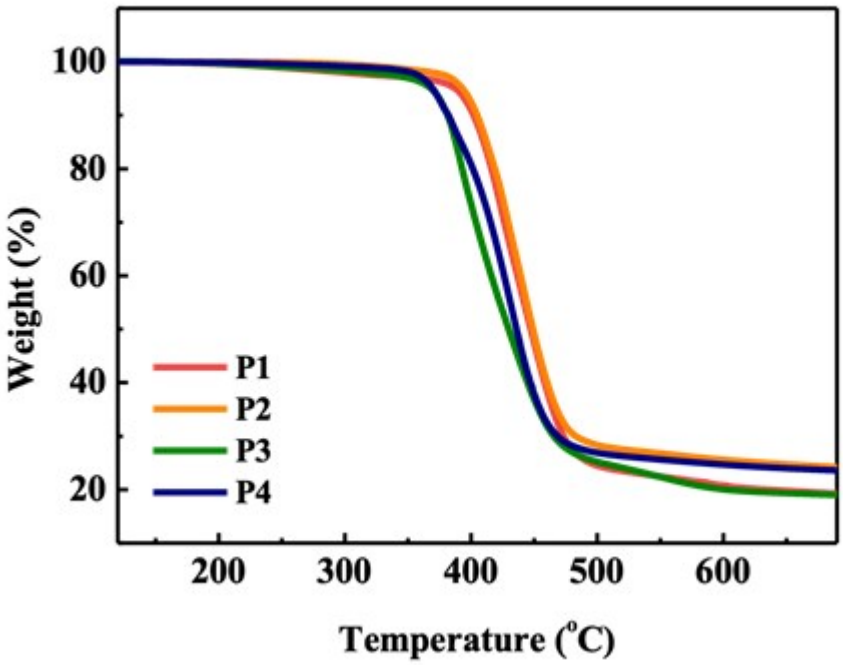

Figure S16. TGA curves of **P1-P4**.

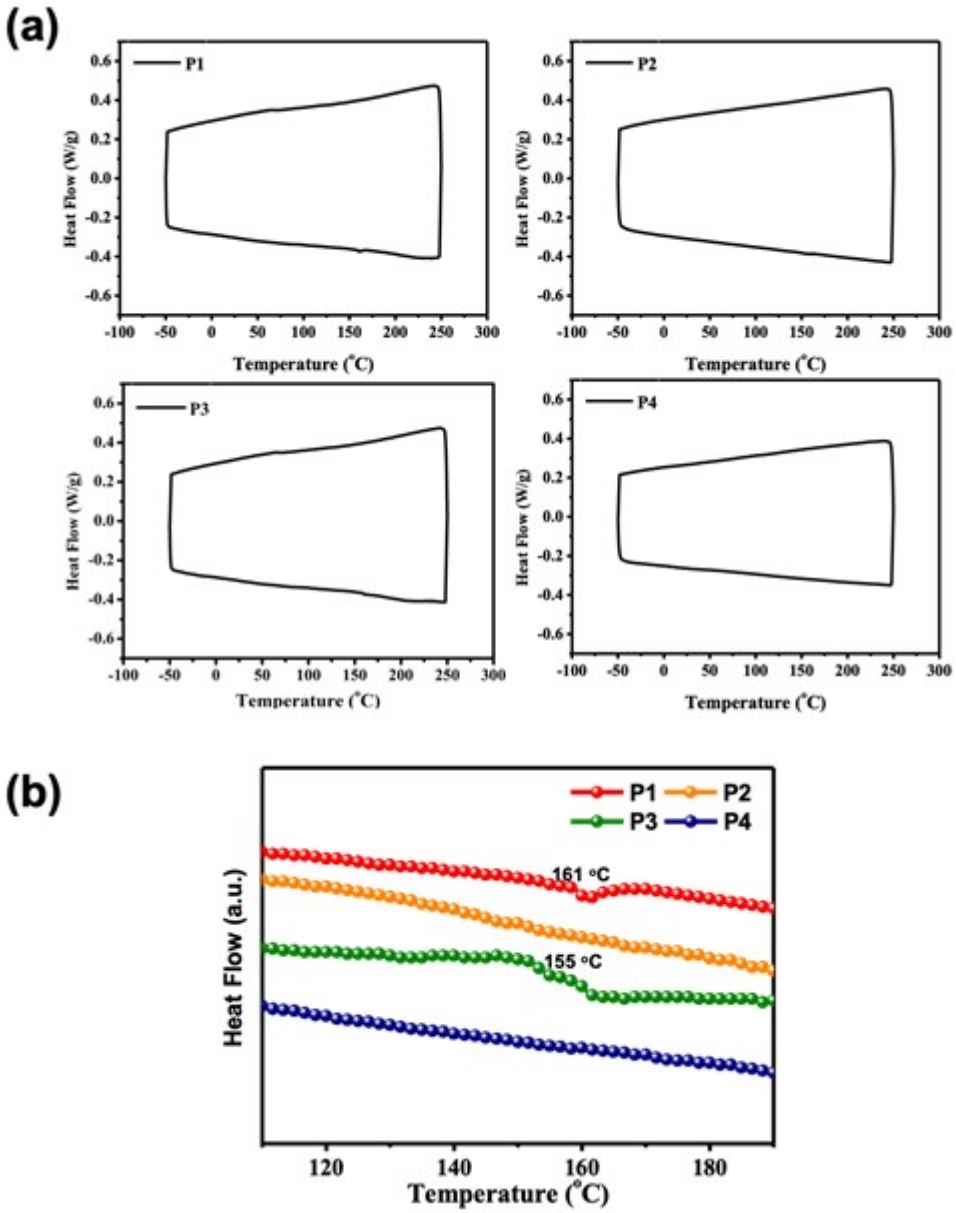

Figure S17. (a) DSC profiles of **P1-P4** in the second heating−cooling cycle. (b) Zoom-in view of the second heating profiles between 100−200 °C for **P1-P4**.

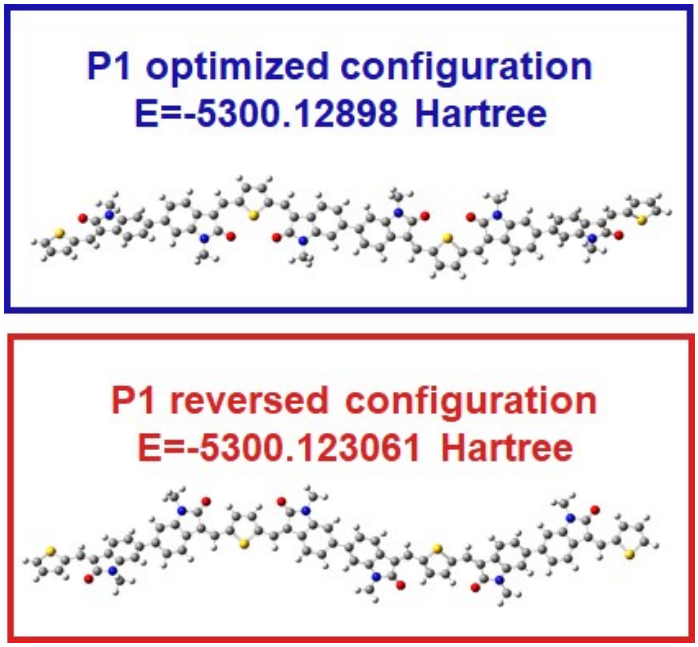

Figure S18. The energy of the reverse and optimized configuration of **P1** predicted by DFT calculation

Table S1. Energy level, reorganization energy, and dipole moment of **P1-P4** predicted by DFT calculation.

	$HOMO_{cal}$[a] (eV)	$LUMO_{cal}$[a] (eV)	$E_{g,DFT}$[a] (eV)	λ_{hole}[a] (meV)	$\lambda_{electron}$[a] (meV)	M[b] (D)
P1	−4.97	−2.73	2.24	167.3	193.4	1.33
P2	−4.99	−2.82	2.17	156.4	217.0	0.47
P3	−4.70	−2.86	1.84	168.0	228.8	0.05
P4	−4.77	−2.95	1.82	168.4	122.0	0.01

[a] HOMO, LUMO, bandgap, electron and hole reorganization energy were predicted by DFT calculation using B3LYP method with 6- 311G(d,p) basic set; [b] Dipole moment of the oligomer chain consisting of three repeating units.

Table S2. The energy of neutral, cation, and anion states of **P1-P4** estimated by DFT calculation.

	Neutral (hartree)			Cation (hartree)		Anion (hartree)	
	−1(N^-)	**0(N_{geo})**	**+1(N^+)**	**0(C_0)**	**+1(C_{geo})**	**0(A_0)**	**−1(A_{geo})**
P1	−3717.82	−3717.75	−3717.54	−3717.75	−3717.54	−3717.75	−3717.82
P2	−5141.03	−5140.96	−5140.75	−5140.96	−5140.75	−5140.95	−5141.03
P3	−3562.97	−3562.9	−3562.7	−3562.9	−3562.7	−3562.9	−3562.97
P4	−4985.51	−4985.39	−4985.18	−4985.39	−4985.18	−4985.39	−4985.51

Table S3. The reorganization energy of **P1-P4** estimated by DFT calculation.

	λ_0 (h^+) (eV)	λ_+ (eV)	λ_{hole} (eV)	λ_0 (e^-) (eV)	λ_- (eV)	$\lambda_{electron}$ (eV)
	C_0-N_{geo}	$(N_+)-C_{geo}$	λ_0 (h+)+λ_+	A_0-N_{geo}	$(N_-)-A_{geo}$	λ_0 (e−)+λ_-
P1	0.0856	0.0817	0.1673	0.1245	0.0689	0.1934
P2	0.0793	0.0770	0.1564	0.1149	0.1022	0.2170
P3	0.0947	0.0733	0.1680	0.1168	0.1060	0.2228
P4	0.0766	0.0918	0.1684	0.0507	0.0712	0.1220

or **Tables S2** and **S3**, λ_- and λ_+ are the geometric relaxation energies on going from the geometry of the neutral state to that of the single-charged radical state. λ_0 is from the geometry of the single-charged radical state to that of the neutral state. A_{geo} and C_{geo} respectively mean the total energy of the optimized anion/cation geometry. N_{geo} represents the total energy of the optimized neutral geometry. A_0 and C_0 respectively are the total energy of anion/cation molecule at the optimized neutral geometry, and N_-, N_+ are the total energy of neutral molecular at the optimized anion/cation radical geometry.

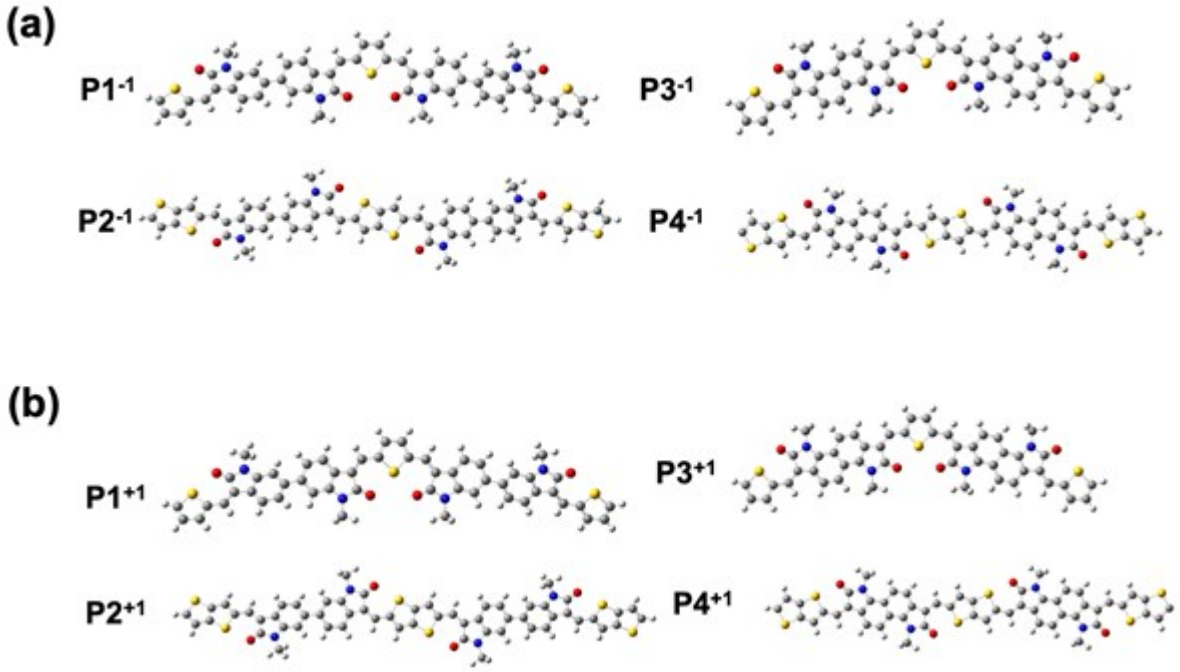

Figure S19. The optimized anion and cation oligomer geometry predicted by DFT calculation.

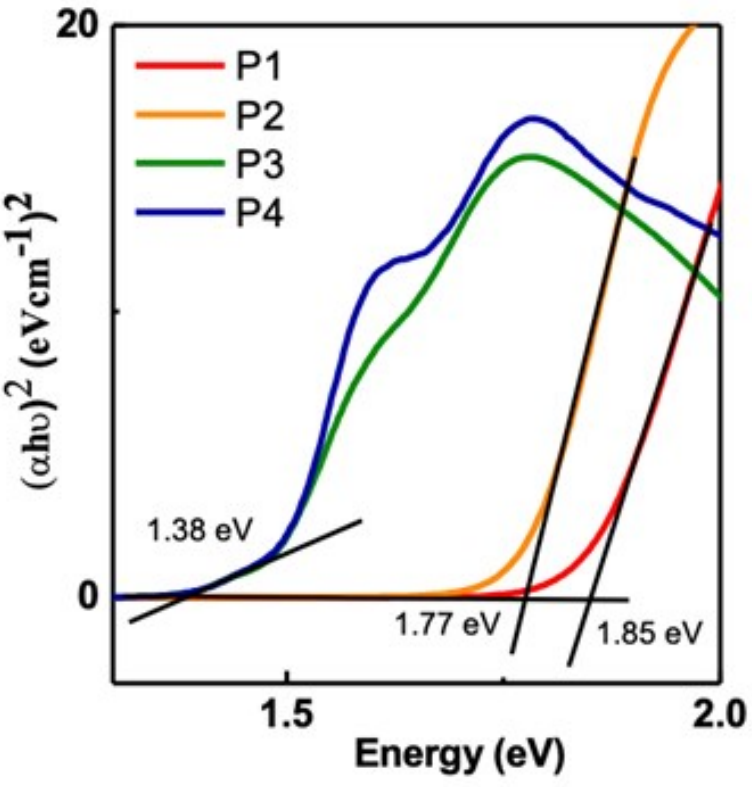

Figure S20. Tauc plots for **P1-P4**.

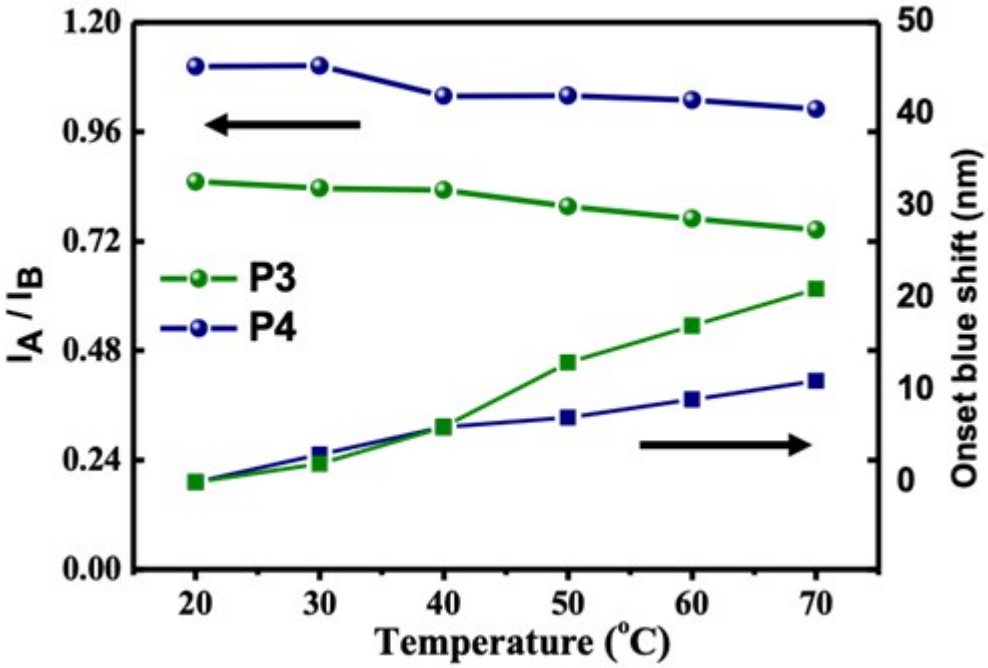

Figure S21. The relationship between the UV−vis absorption attenuation and the absorption band shifting of **P3** and **P4** with various temperature.

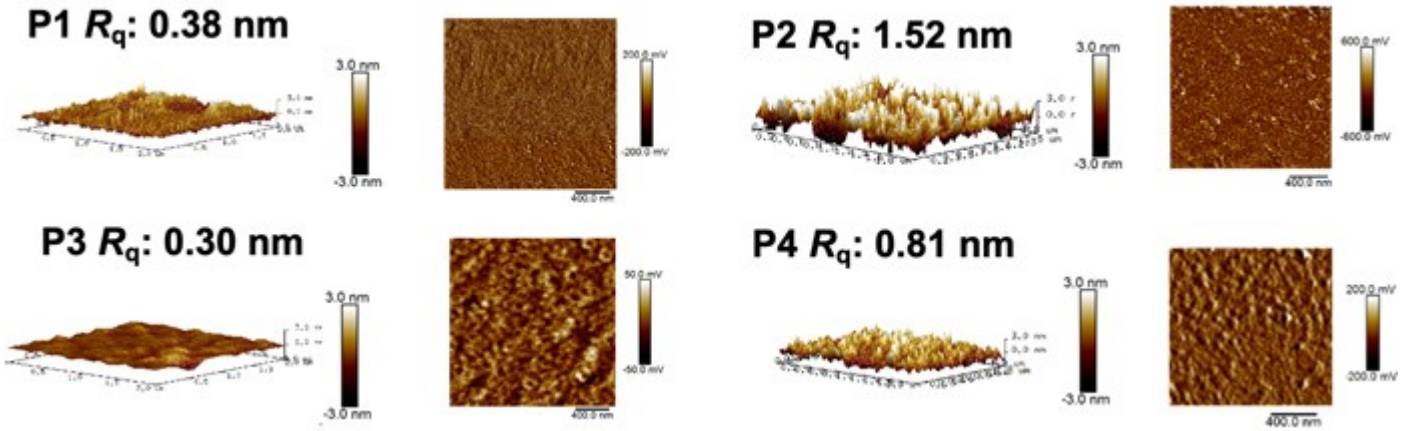

Figure S22. AFM 3D-height images and phase images of the as-cast polymer films based on **P1-P4**.

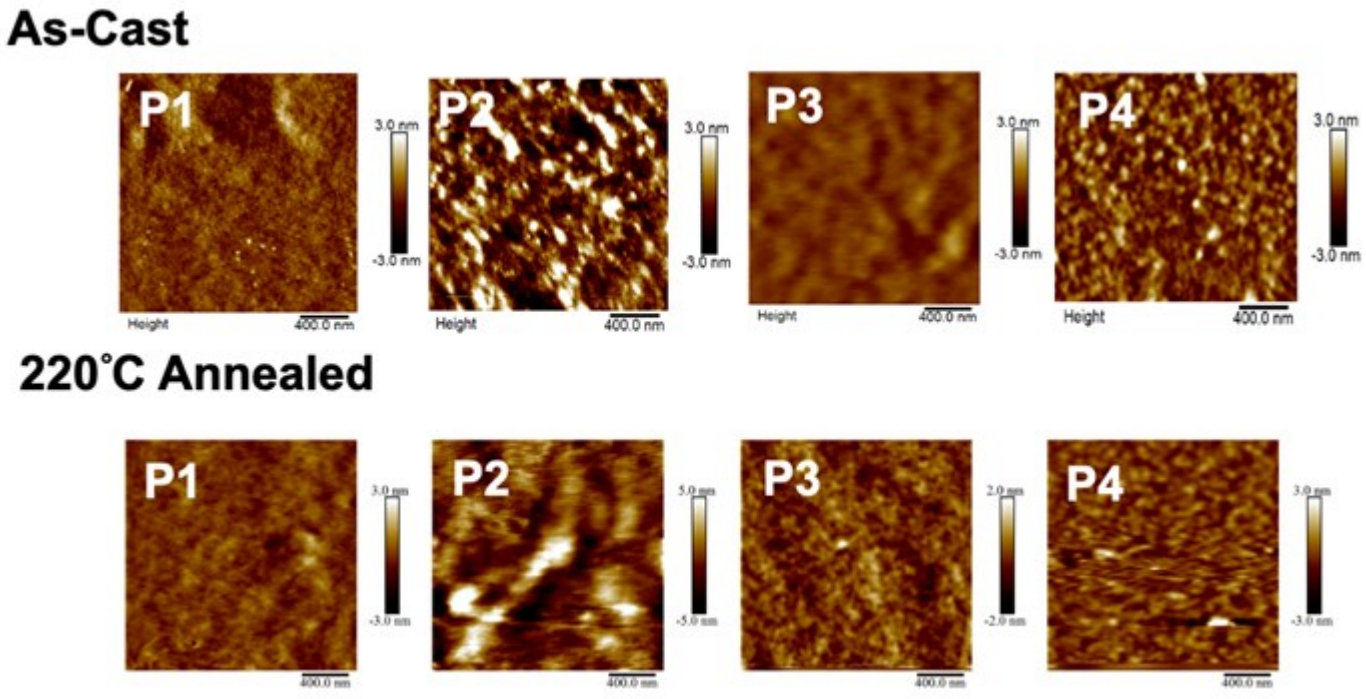

Figure S23. Comparison of AFM topographies of the as-cast and annealed films of **P1-P4**.

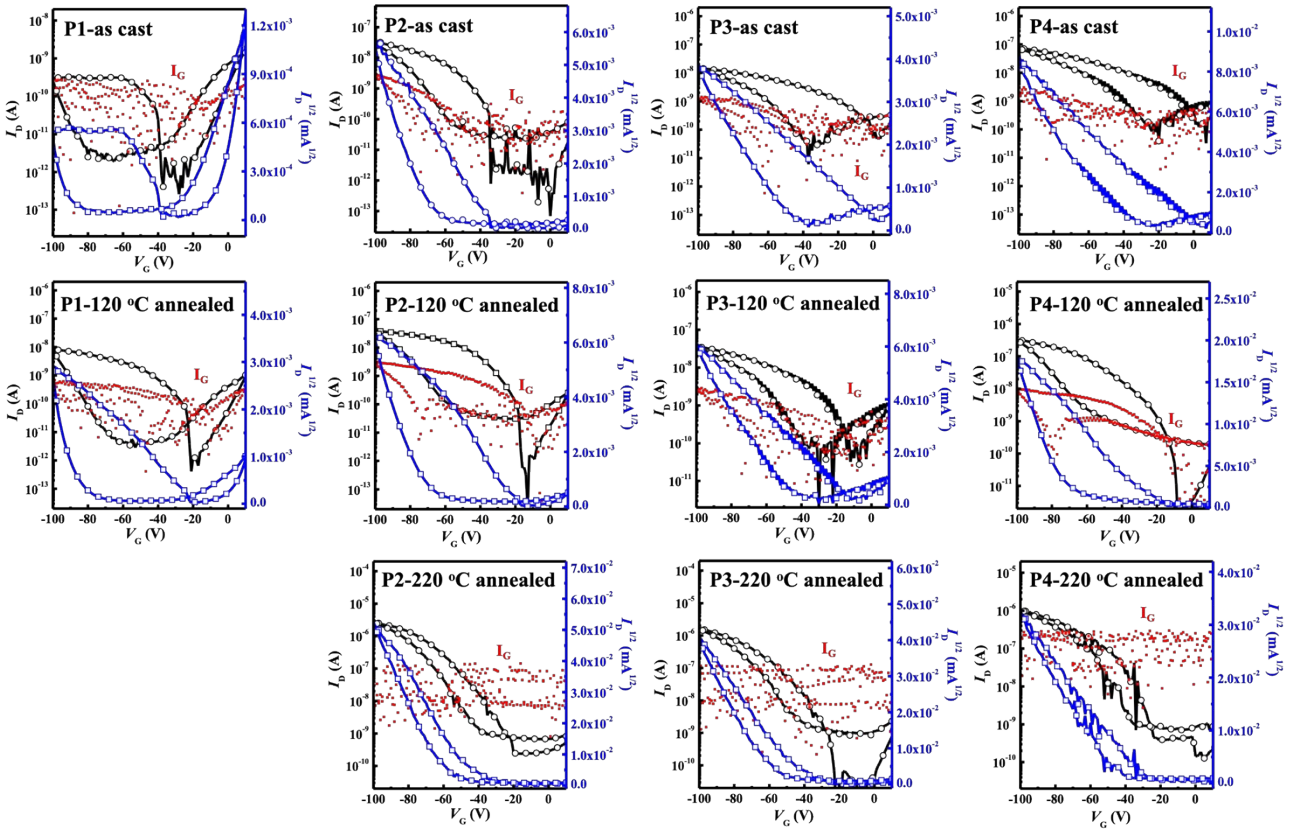

Figure S24. P-type FET transfer characteristics of the films of **P1-P4** under varied annealing temperatures. [black curve: drain current (I_D) and red dots: gate leakage current (I_G)]

Table S4. P-type FET device characteristics of the films of **P1-P4** under varied annealing conditions.

	$T_{Annealing}$ (°C)	μ_h (cm² V⁻¹ s⁻¹)[a]	$\mu_{h,max}$ (cm² V⁻¹ s⁻¹)	I_{on}/I_{off}	V_{th} (V)
P1	As-cast	$7.4 \times 10^{-7} \pm 2 \times 10^{-7}$	9.5×10^{-7}	7×10^{4}	−15
	120	$1.9 \times 10^{-5} \pm 8 \times 10^{-6}$	3.5×10^{-5}	1×10^{5}	−29
	220	––	––	––	––
P2	As-cast	$9.3 \times 10^{-5} \pm 2 \times 10^{-5}$	1.1×10^{-4}	3×10^{5}	-32
	120	$1.1 \times 10^{-4} \pm 4 \times 10^{-5}$	1.4×10^{-4}	6×10^{5}	−16
	220	$7.0 \times 10^{-3} \pm 3 \times 10^{-3}$	0.011	2×10^{5}	−35
P3	As-cast	$1.7 \times 10^{-5} \pm 1 \times 10^{-5}$	3.2×10^{-5}	3×10^{2}	−3
	120	$4.5 \times 10^{-5} \pm 2 \times 10^{-5}$	6.2×10^{-5}	1×10^{3}	−8
	220	$3.6 \times 10^{-3} \pm 1 \times 10^{-3}$	5.8×10^{-3}	8×10^{5}	−35
P4	As-cast	$8.4 \times 10^{-5} \pm 7 \times 10^{-6}$	9.2×10^{-5}	3×10^{3}	−5
	120	$7.6 \times 10^{-4} \pm 5 \times 10^{-4}$	1.3×10^{-3}	1×10^{6}	−21
	220	$1.7 \times 10^{-3} \pm 5 \times 10^{-4}$	2.5×10^{-3}	2×10^{5}	−24

[a] At least 20 devices from 3 different batches were acquired for the average FET characteristics.

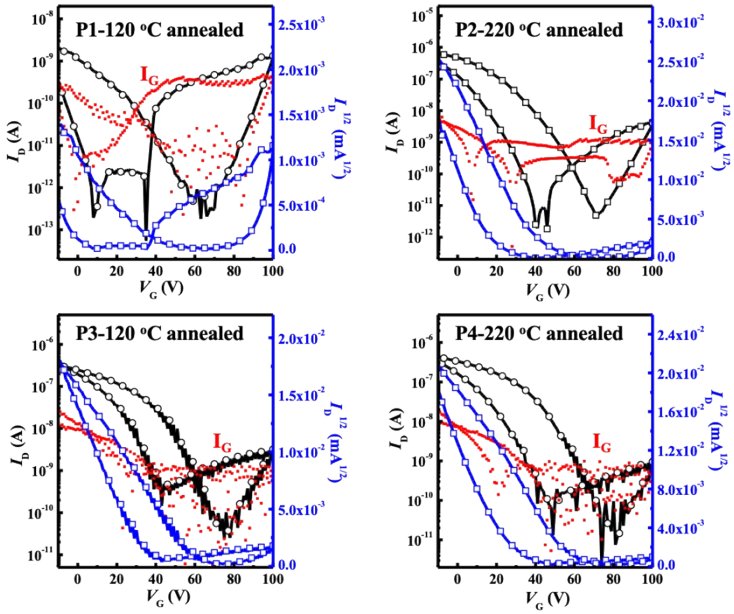

Figure S25. N-type FET transfer characteristics of the films of **P1-P4**. [black curve: drain current (I_D) and red dots: gate leakage current (I_G)]

Table S5. N-type FET device characteristics of the films of **P1-P4**.

	$T_{Annealing}$ (°C)	μ_e[a] (cm^2 V^{-1} s^{-1})	$\mu_{e,max}$ (cm^2 V^{-1} s^{-1})	I_{on}/I_{off}	V_{th} (V)	μ_h/μ_e
P1	120	$8.6 \times 10^{-6} \pm 1 \times 10^{-6}$	1.0×10^{-5}	2×10^5	40	2.2
P2	220	$1.3 \times 10^{-5} \pm 9 \times 10^{-6}$	2.3×10^{-5}	2×10^5	46	539
P3	220	$8.9 \times 10^{-6} \pm 8 \times 10^{-6}$	1.4×10^{-5}	9×10^4	31	405
P4	220	$1.6 \times 10^{-6} \pm 1 \times 10^{-6}$	2.1×10^{-6}	3×10^4	23	1063

[a] At least 20 devices from 3 different batches were acquired for the average FET characteristics.

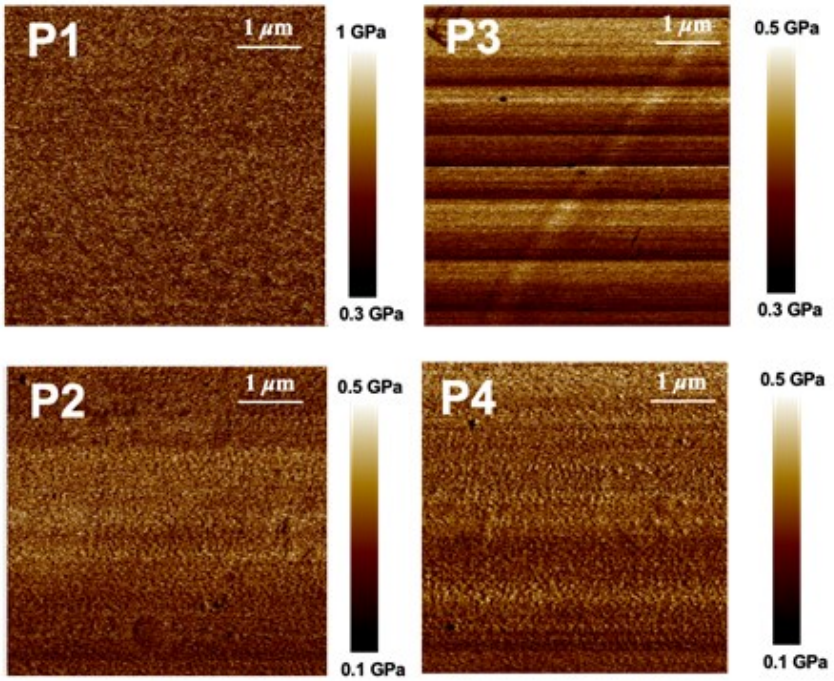

Figure S26. AFM surface mechanical mapping of the polymer films.

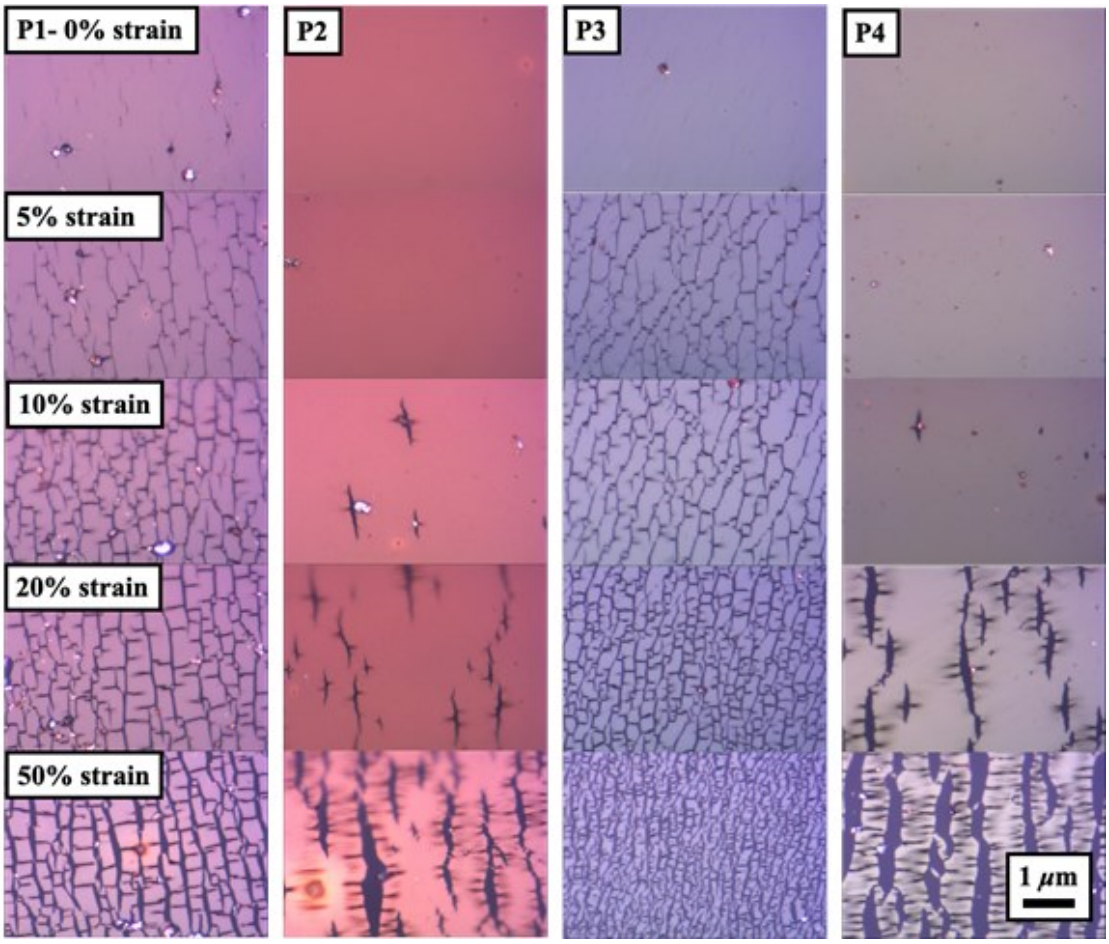

Figure S27. OM images of the transferred and stretched polymer films with external strains ranging from 0 to 50%.

References

(1) Ganguly, A.; He, K.; Hendsbee, A. D.; Abdelsamie, M.; Bennett, R. N.; Li, Y.; Toney, M. F.; Kelly, T. L., Synthesis of Poly(bisisoindigo) Using a Metal-Free Aldol Polymerization for Thin-Film Transistor Applications. *ACS Appl Mater Interfaces* **2020,** 12, 12, 14265-14271.

(2) Onwubiko, A.; Yue, W.; Jellett, C.; Xiao, M.; Chen, H. Y.; Ravva, M. K.; Hanifi, D. A.; Knall, A. C.; Purushothaman, B.; Nikolka, M.; Flores, J. C.; Salleo, A.; Bredas, J. L.; Sirringhaus, H.; Hayoz, P.; McCulloch, I., Fused electron deficient semiconducting polymers for air stable electron transport. *Nat. Commun.* **2018,** 9, 1, 416.

(3) Randell, N. M.; Boutin, P. C.; Kelly, T. L., Bisisoindigo: using a ring-fusion approach to extend the conjugation length of isoindigo. *J. Mater. Chem. A* **2016,** 4, 18, 6940-6945.

(4) Randell, N. M.; Radford, C. L.; Yang, J.; Quinn, J.; Hou, D.; Li, Y.; Kelly, T. L., Effect of Acceptor Unit Length and Planarity on the Optoelectronic Properties of Isoindigo–Thiophene Donor–Acceptor Polymers. *Chem. Mater.* **2018,** 30, 14, 4864-4873.